JOURNAL OF SOLID STATE CHEMISTRY 102, 164–174 (1993)

Structure–Property Relationships in the Layered Cuprate $La_{2-x}Sr_xCuSnO_6$

MARK T. ANDERSON AND KENNETH R. POEPPELMEIER*

Department of Chemistry and the Science and Technology Center for Superconductivity, Northwestern University, Evanston, Illinois 60208

AND STEPHEN A. GRAMSCH AND JEREMY K. BURDETT*

Department of Chemistry, the James Franck Institute, and the Science and Technology Center for Superconductivity, University of Chicago, Chicago, Illinois 60637

Received April 20, 1992; accepted June 24, 1992

In an attempt to induce a metallic or superconductive state in the layered cuprate La_2CuSnO_6, the series $La_{2-x}Sr_xCuSnO_{6-x/2+\delta}$ (x = 0.00, 0.05, 0.10, 0.125, 0.15, 0.175, 0.20) was prepared. A solid solution forms for $0.00 < x < 0.175$, the overall oxygen content is 6.00 (3), and the samples are antiferromagnetic semiconductors. From neutron diffraction experiments, the compounds possess distinct copper–oxygen and tin–oxygen layers. There is a mismatch at the interface of the layers, which results in expansion of the copper–oxygen bond lengths (1.99 Å average). The copper is oxidized upon addition of strontium; however, in contrast to *p*-type cuprate superconductors, the in-plane copper–oxygen bond lengths *increase* and the axial bonds *decrease*. The interleaved tin–oxygen layers have a dramatic effect on the crystal chemistry, electronic structure, and properties. The electronic consequence is that empty upper and filled lower $dx^2 - y^2$ bands (upper and lower Hubbard bands) remain separated and narrow upon oxidation, which presumably prohibits superconductivity. © 1993 Academic Press, Inc.

Introduction

Layered copper-oxide superconductors exhibit the highest critical transition temperatures of any materials. The maximum transition temperatures are achieved for compounds that contain dopant-free copper–oxygen layers and that have been chemically modified to formally oxidize or reduce a fraction of the copper. The synthesis and chemical modification (oxidation or reduction) of new compounds that contain small nonmagnetic B'' ions between—rather than within—the copper-oxide layers is our goal. Compounds of this type, such as La_2CuSnO_6 (*1*), provide crystal chemistry and electronic structures different from simple cuprate superconductors and should offer advantages in the study of the physics and chemistry that underlie superconductivity. A common way to modify physical properties of such compounds is to substitute a cation onto a crystallographic site not occupied by copper, for example, $La_{2-x}Sr_xCuO_{4-x/2+\delta}$ (*2*, *3*), $Nd_{2-x}Ce_xCuO_{4+x/2-\delta}$ (*4*),

[1] To whom correspondence should be addressed.

0022-4596/93 $5.00

Copyright © 1993 by Academic Press, Inc.
All rights of reproduction in any form reserved.

$La_{2-x}Sr_xCaCu_2O_{6+y}$ (*5*), and $Y_{1-x}Ca_xSr_2Cu_2GaO_{7-x/2+\delta}$ (*6*). In this work, we detail the crystal chemistry bulk physical properties of the series $La_{2-x}Sr_xCuSnO_{6-x/2+\delta}$ and focus on the effect that tin has on the structure–property relationships.

Experimental

Sample Preparation

$La_{2-x}Sr_xCuSnO_{6-x/2+\delta}$ (x = 0.00, 0.05, 0.10, 0.125, 0.15, 0.175, and 0.20) samples were prepared by the solid-state reaction of lanthanum oxide (99.99%), strontium carbonate (99.999%), tin(IV) oxide (99.995 + %), and copper(II) oxide (99.999%). The lanthanum oxide was heated in air before use and cooled in a desiccator to remove any trace of water or carbonate. The reagents were ground and fired in high-density alumina boats for one day. The samples were then quenched in air, ground, pressed into pellets, and fired at 980°C in air. The process was repeated several times. At this temperature, a minimum reaction time of about 21 days was required to achieve a single phase. All measurements made were performed on samples prepared in air unless otherwise noted. A portion of each sample was annealed at 400°C in flowing oxygen for 12 hr and slowly cooled to room temperature. A portion of the quenched x = 0.10, 0.15, and 0.20 samples was annealed under 215 bars oxygen at 600°C for about 8 hr and slowly cooled to room temperature, and the x = 0.125 and 0.175 samples were annealed under 200 bars oxygen at 910°C for about 8 hr and slowly cooled to room temperature.

Powder X-ray Diffraction

An X-ray diffraction data set suitable for Rietveld (*7*) refinement was collected for each sample. A Rigaku diffractometer with nickel-filtered Cu$K\alpha$ radiation was used to collect the data. Silicon (99.9999%) was used as an internal standard. Data were collected from 10 to 80° 2θ with a step of 0.02° and a collection time of 10 sec at each step. A 50-kv acceleration voltage and 20-mA excitation current were used. Rietveld techniques were used to determine the lattice constants for each sample.

Neutron Diffraction

The Intense Pulsed Neutron Source at Argonne National Laboratory was used to collect time-of-flight data on a 7-g polycrystalline sample of $La_{1.85}Sr_{0.15}CuSnO_6$. Data were collected for 6 hr on a sample that was at room temperature and ambient pressure. The data set from d = 0.623 to 2.970 Å was analyzed by Rietveld methods (*8, 9*). Sixty-four parameters were refined, which included scale factor, diffractometer constant, zero-point error, background, peak shape, unit cell and positional parameters, isotropic thermal factors, and absorption and extinction parameters. The coherent scattering lengths used for La, Sr, Cu, Sn, and O were 8.24, 7.02, 7.72, 6.23, and 5.80 fm, respectively (*10*).

Susceptibility Measurements

A Quantum Design Corporation MPMS SQUID susceptometer was employed to record magnetic data. Data were collected with a 1-kG applied field between 5 and 300 K. The measurements were performed on finely ground samples that were contained in sealed gelatin capsules. The data were corrected for the diamagnetism of the sample holder. A platinum metal standard was used to calibrate the instrument.

Resistivity Measurements

Four-probe resistivity measurements were performed on sintered polycrystalline samples x = 0.00 and 0.15. Copper leads were attached with silver paint. A constant excitation current of 2.5 μA was applied for the former sample and 100 μA for the latter sample. Resistance was monitored with a

digital multimeter. Data were recorded from 300 to 240 K for $x = 0.00$ and 300 to 80 K for $x = 0.15$.

Thermogravimetric Analysis

A DuPont 9900 thermogravimetric analysis system was used to determine oxygen content. Samples were heated from 25 to 1050°C at 10°/min under a 30 cc/min flow of 8.5% hydrogen in helium. At least two runs were performed for each sample. A profile of the empty platinum pan was recorded before each run and was subtracted from the profile of the sample.

Mössbauer Spectroscopy

Mössbauer Spectroscopy Consultants provided ^{119}Sn analyses of $x = 0.00$ and 0.15. Data were collected for about 12 hr on each sample. $BaSnO_3$ was used as a reference material.

Results

Solid Solution and Structure

Strontium is soluble in $La_{2-x}Sr_xCuSnO_{6-x/2+\delta}$ in the range $0.00 < x < 0.175$; an impurity of $SrSnO_3$ is present in the $x \geq 0.175$ diffraction patterns. Figure 1 demonstrates that the b and c lattice parameters increase up to $x = 0.175$ and the a lattice parameter decreases linearly from $x = 0.00$ to $x = 0.175$. The overall unit cell volume remains nearly the same. No extension of the solubility limit was observed for the samples annealed under high oxygen pressure.

The structure of $La_{1.85}Sr_{0.15}CuSnO_6$ was refined by Rietveld analysis of neutron diffraction data. The structure of the undoped material served as a model (*1*). The refinement converged to reliability factors (*11*) $R_p = 2.9\%$, $R_{wp} = 4.4\%$, $R_{|F|^2} = 4.2\%$, $R_{\text{Riet}} = 7.8\%$ with $R_{\text{exp}} = 2.6\%$. The atomic positions and other crystallographic information are presented in Table I. The ob-

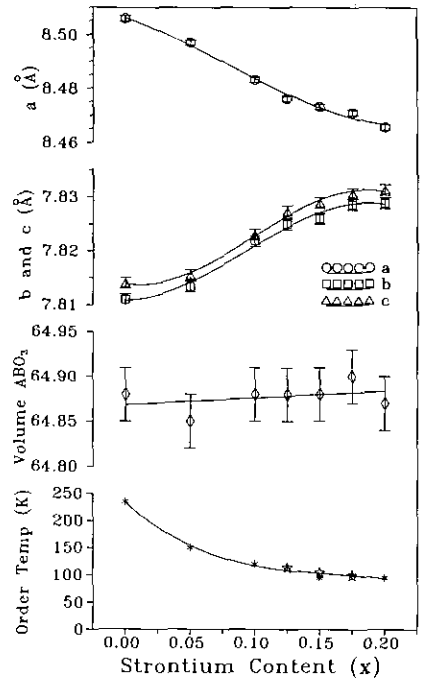

FIG. 1. Lattice constants, volume per perovskite unit (ABO_3), and maximum temperature at which antiferromagnetic order exists versus strontium content for $La_{2-x}Sr_xCuSnO_6$. Magnetic measurements were performed on samples that were quenched in air (*) and that were slowly cooled under high oxygen pressure (★).

served, calculated, and difference patterns and allowed reflections are displayed in Figure 2. The A–O bond distances are shown in Table II. Complete list of B–O distances and their changes from La_2CuSnO_6 are presented in Table III. A labeled view of the structure appears in Fig. 3.

The important differences relative to the parent are the increase of the in-plane Cu–O bond lengths (*12*), the decrease in axial Cu–O bond lengths, and the slightly flattened $CuO_{4/2}$ and $SnO_{4/2}$ planes. The longer copper oxygen bonds and the flattened copper–oxygen planes result in an increase of the b and c lattice parameters. Similarly, the decreased axial bond lengths result in a decrease of the a lattice parameter.

TABLE I

CRYSTALLOGRAPHIC DATA FOR $La_{1.85}Sr_{0.15}CuSnO_6$[a]

Atom	Site	$x/\mathbf{a}$ (σx)	$y/\mathbf{b}$ (σy)	$z/\mathbf{c}$ (σz)	B(Å^2)(σB)	Occupancy
La1/Sr1	2*e*	0.2126(5)	$\frac{1}{4}$	0.2808(7)	0.72(9)	0.925–0.075
La2/Sr2	2*e*	0.2010(5)	$\frac{1}{4}$	0.7696(7)	0.59(8)	0.925–0.075
La3/Sr3	2*e*	0.7565(5)	$\frac{1}{4}$	0.7838(6)	0.74(9)	0.925–0.075
La4/Sr4	2*e*	0.7694(5)	$\frac{1}{4}$	0.2743(6)	0.82(9)	0.925–0.075
Cu1	2*a*	0	0	0	0.66(8)	1
Cu2	2*c*	0	0	$\frac{1}{2}$	0.34(8)	1
Sn1	2*b*	$\frac{1}{2}$	0	0	0.22(9)	1
Sn2	2*d*	$\frac{1}{2}$	0	$\frac{1}{2}$	0.48(10)	1
O1	4*f*	0.0350(4)	−0.0307(5)	0.2501(5)	0.34(7)	1
O2	4*f*	0.2677(4)	−0.0472(6)	−0.0485(6)	0.69(8)	1
O3	4*f*	0.2729(4)	0.0502(6)	0.5518(6)	0.84(8)	1
O4	4*f*	0.4314(4)	0.0454(5)	0.2498(6)	0.69(8)	1
O5	2*e*	0.0280(7)	$\frac{1}{4}$	0.0321(8)	0.86(10)	1
O6	2*e*	0.4603(7)	$\frac{1}{4}$	−0.0745(7)	0.92(11)	1
O7	2*e*	0.5804(6)	$\frac{1}{4}$	0.5244(7)	0.27(9)	1
O8	2*e*	−0.0173(6)	$\frac{1}{4}$	0.4727(7)	0.09(10)	1

[a] Space group $P2_1/m$ with a = 8.4735(10), b = 7.8322(9), c = 7.8336(9) Å, β = 91.005(1)°, and Z = 4.

Redox Chemistry

Thermogravimetric analysis (TGA) on each sample ($0.00 \leq x \leq 0.15$) indicated no statistically significant deviation from an overall oxygen content of 6.00, as shown in Fig. 4. The overall reaction is

$$La_{2-x}Sr_xCuSnO_{6-x/2+\delta} + (3 - x + \delta)H_2 \rightarrow 1 - (x/2)La_2O_3 + x/2\ Sr_2SnO_4 + 1 - (x/2)Sn^0 + Cu^0 + (3 - x + \delta)H_2O\uparrow. \quad (1)$$

The presence of Sn^0 and Sr_2SnO_4 was confirmed by X-ray diffraction. An equal mixture of the two products was observed when $SrSnO_3$ was reduced in a hydrogen/helium mixture. Strontium is quite electropositive, therefore it stabilizes tin(IV) in the highly reducing atmosphere. From the TGA results, we conclude that an amount of copper(II) equal to the amount of strontium (x) is oxidized to copper(III), and the amount of oxygen incorporated into the structure from the air during synthesis (δ) is equal to one-half the strontium content ($x/2$) for all values of x.

Mössbauer spectroscopy confirmed that the tin is exclusively tetravalent in the x = 0.00 and 0.15 samples. The isomer shift relative to $BaSnO_3$ is 0.09 mm/sec for x = 0.00 and 0.11 mm/sec for x = 0.15. There is a small quadropole splitting for both samples (0.70 and 0.71, respectively).

Properties

The moments on the copper atoms in La_2CuSnO_6 are antiferromagnetically coupled and display an order temperature of about 230 K. The maximum in magnetic susceptibility versus temperature is broad, which is characteristic of two-dimensional order. The strength of the magnetic interactions decreases as strontium is introduced, as shown in Fig. 1. The maximum remains quite broad and the magnetic interactions persist even at x = 0.15; see Fig. 5. The figure also illustrates the difference in profiles when the sample is field cooled versus zero field cooled.

La_2CuSnO_6 is an intrinsic semiconductor. A plot of log conductivity versus inverse

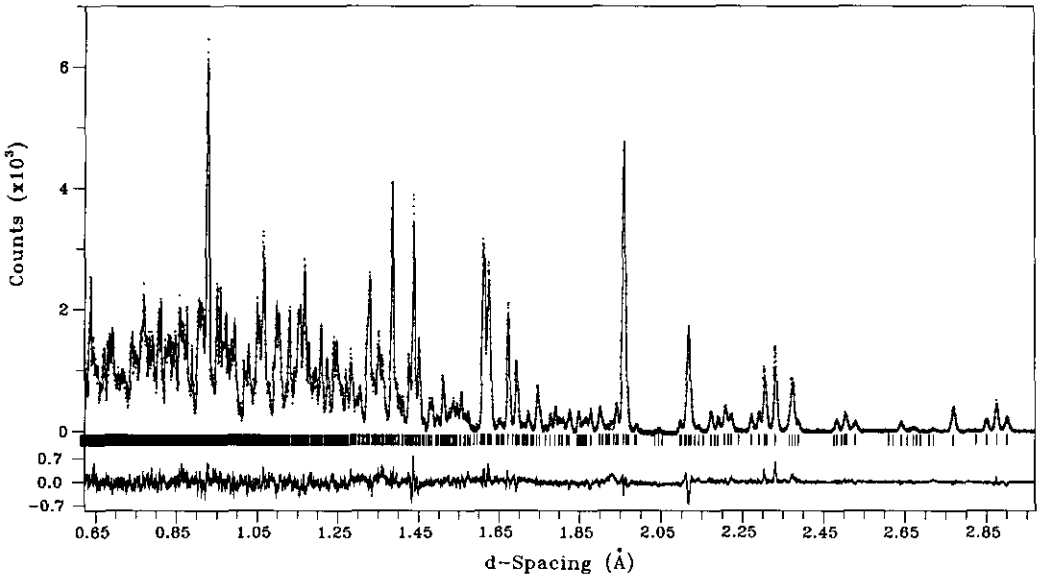

FIG. 2. Observed (+), calculated (solid line) and difference (below) neutron diffraction pattern for $La_{2-x}Sr_xCuSnO_6$. The tic marks indicate the allowed reflections in space group $P2_1/m$.

temperature, shown in Fig. 6, is linear. The activation energy is about 0.3 eV, and the resistivity at room temperature is about 2000 Ω · cm. $La_{1.85}Sr_{0.15}CuSnO_6$ appears to be a heavily doped semiconductor. The activation energy is about 0.08 eV, and the resistivity at room temperature is about 50 Ω · cm.

TABLE II

A–O BOND DISTANCES[a] IN $La_{1.85}Sr_{0.15}CuSnO_6$

La1/Sr1 –O4	2.467(5) × 2	La3/Sr3 –O1	2.482(5) × 2
–O5	2.476(8)	–O7	2.500(7)
–O8	2.481(7)	–O2	2.623(6) × 2
–O1	2.672(4) × 2	–O6	2.762(7)
–O3	2.679(6) × 2	–O4	2.818(5) × 2
		–O5	2.986(8)
		–O8	3.127(7)
La2/Sr2 –O3	2.401(6) × 2	La4/Sr4 –O8	2.363(7)
–O6	2.495(7)	–O2	2.394(6) × 2
–O5	2.547(8)	–O7	2.552(7)
–O1	2.639(5) × 2	–O3	2.744(5) × 2
–O2	2.782(5) × 2	–O5	2.923(8)
–O8	2.946(7)	–O1	3.155(6) × 2
		–O4	3.284(5) × 2

[a] For oxygen atoms within 3.5 Å. Bond distances in angstroms.

Related Systems

No evidence of superconductivity was observed in $La_{2-x}M_xCuSnO_{6-x/2+\delta}$ (M = Ca, Sr, Ba; $0 \leq x \leq 0.40$). Each material was screened with an ac susceptometer, which was calibrated with the superconductor $YBa_2Cu_3O_{7-y}$. In the calcium-doped samples, the increases of the b and c lattice parameters are less than for the strontium-doped samples; however, the magnetic order temperatures are consistently higher than for the strontium doped samples. Figure 7 summarizes the structural and magnetic data for the calcium-doped series.

The following systems have been investigated in an attempt to alter the crystal chemistry and physical properties of La_2CuSnO_6. Each resulted in mixture of several phases for every value of x. The target compounds were $La_2CuSn_{1-x}Al_xO_6$ (p-type), $La_{2-x}Ce_xCuSnO_6$ and $La_2CuSn_{1-x}Sb_xO_6$ (n-type), and $La_2CuSn_{1-x}Ti_xO_6$ (isoelectric). The isoelectric substitution

TABLE III

B–O BOND DISTANCES[a] AND ANGLES FOR $La_{1.85}Sr_{0.15}CuSn_6$[b] AND THEIR CHANGES FROM La_2CuSnO_6

Bond		Distance	Change	Bond	Angle	Change
Cu1	–O5	1.988(1)	0.003	O1–Cu1–O2	89.3(2)	–0.7
	–O1	1.991(4)	0.003	O1–Cu1–O5	88.8(2)	–0.1
	–O2	2.336(3)	–0.031	O2–Cu1–O5	86.4(2)	0.6
Cu2	–O8	1.975(1)	0.004	O1–Cu2–O3	88.5(2)	0.3
	–O1	2.000(4)	–0.003	O1–Cu2–O8	88.5(2)	–0.1
	–O3	2.373(4)	–0.022	O3–Cu2–O8	85.6(2)	–0.2
Sn1	–O2	2.032(3)	0.007	O2–Sn1–O4	85.5(2)	0.6
	–O6	2.069(2)	0.001	O2–Sn1–O6	88.1(2)	–0.7
	–O4	2.081(4)	0.000	O4–Sn1–O6	86.8(2)	0.2
Sn2	–O3	2.013(4)	–0.010	O3–Sn2–O4	84.5(2)	–0.5
	–O4	2.066(4)	0.000	O3–Sn2–O7	83.7(2)	0.4
	–O7	2.081(2)	–0.002	O4–Sn2–O7	89.4(2)	0.3
				Cu1–O1–Cu2	157.9(2)	1.1
				Cu1–O2–Sn1	151.8(2)	0.6
				Cu2–O3–Sn2	149.9(2)	1.2
				Sn2–O4–Sn1	141.6(2)	0.7
				Cu1–O5–Cu1	160.2(4)	0.5
				Sn2–O6–Sn1	142.6(2)	0.8
				Sn2–O7–Sn2	140.4(3)	1.0
				Cu2–O8–Cu2	165.1(3)	0.5

[a] For oxygen atoms within 3.5 Å.
[b] Bond distances in angstroms and bond angles in degrees.

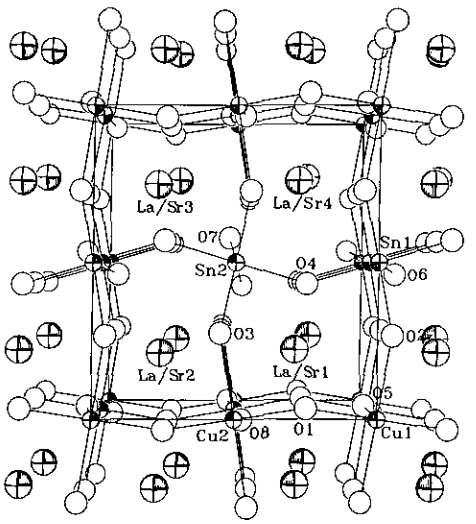

FIG. 3. Structure of $La_{1.85}Sr_{0.15}CuSnO_6$ viewed down the b axis. The filled circles are cations, and the open circles are anions.

was an attempt to decrease the average bond length in the tin–oxygen layers and allow the copper–oxygen bond lengths to shorten.

Discussion

Crystal Chemistry

The structure of $La_{1.85}Sr_{0.15}CuSnO_6$ is very similar to the parent and is best described as a $2a_p \times 2a_p \times 2a_p$ distorted perovskite that contains distinct copper-oxygen and tin-oxygen layers. Two types of cation size mismatches are present in the compound: (1) *A* cation–*B* cation and (2) copper–tin. The first mismatch is three-dimensional and places the Cu–O and Sn–O bonds under compressive stress and places the La–O bonds under tensile stress. The mismatch can be quantified in terms of the Goldschmidt (*13*) tolerance factor adapted for $A_2B'B''O_6$ compounds

$$t = (r_A + r_O)/\sqrt{2}(((r_{B'} + r_{B''})/2) + r_O), \quad (2)$$

in which r_A, r_O, $r_{B'}$, and $r_{B''}$ are the ionic radii (*14*) of the ions. A value less than unity implies the *B*–O bonds are under compression and the *A*–O bonds are under tension. The value for La_2CuSnO_6 is 0.930. The stress on the bonds is partly relieved by tilts

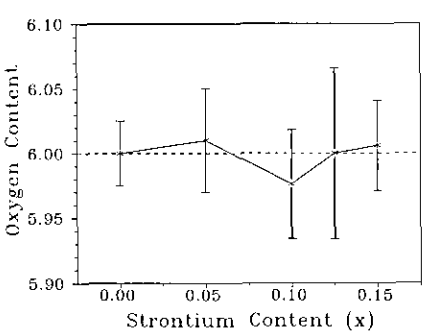

FIG. 4. Total oxygen content versus strontium content for $La_{2-x}Sr_xCuSnO_6$. The error bars are the standard deviation of at least two determinations.

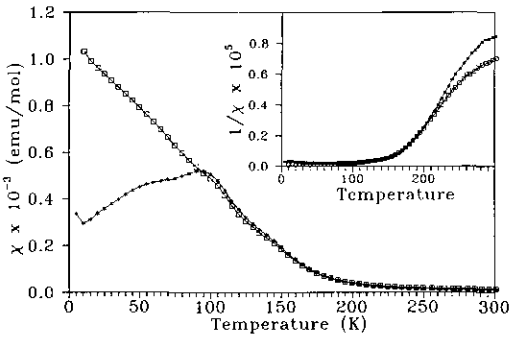

FIG. 5. Magnetic susceptibility versus temperature for $La_{1.85}Sr_{0.15}CuSnO_6$ when field cooled (□) and zero field cooled (*). The inset shows reciprocal susceptibility versus temperature for both samples.

of the BO_6 octahedra. The tilts within the metal–oxygen framework are denoted $a^-b^+c^-$ in the notation introduced by Glazer (*15*). A polyhedral representation of the structure, as viewed down each of the principal axes, is shown in Fig. 8. The tilts reduce the coordination number of each lanthanum from 12 (4 + 4 + 4), found in an ideal perovskite, to 8 for La1 (4 + 2 + 2), 9 for La2 (4 + 4 + 1), 10 for La3 (4 + 2 + 4), and 9 for La4 (4 + 4 + 1) (*16*). The tilts also buckle the copper–oxygen and tin–oxygen planes.

The second mismatch is two-dimensional and compromises the metal–metal and metal–oxygen distances in the tin- and copper–oxygen nets. The mismatch (*17*) across the interface of the two nets is accommodated by a compression of the tin–oxygen net and an expansion of the copper–oxygen net. The metal–metal distance is about 3.90 Å within both nets. The additional compressive stress on the tin–oxygen octahedra causes them to further tilt about [010] and [001]. The tensile stress on the copper–oxygen octahedra causes a decrease in their tilt angle, and elongates the in-plane copper–oxygen bonds (to an average 1.99 Å), but, as a result of the *A–B* mismatch, the layers remain buckled.

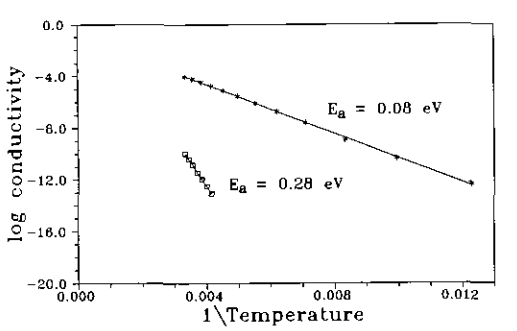

FIG. 6. Log conductivity versus reciprocal temperature for La_2CuSnO_6 (*) and $La_{1.85}Sr_{0.15}CuSnO_6$ (□).

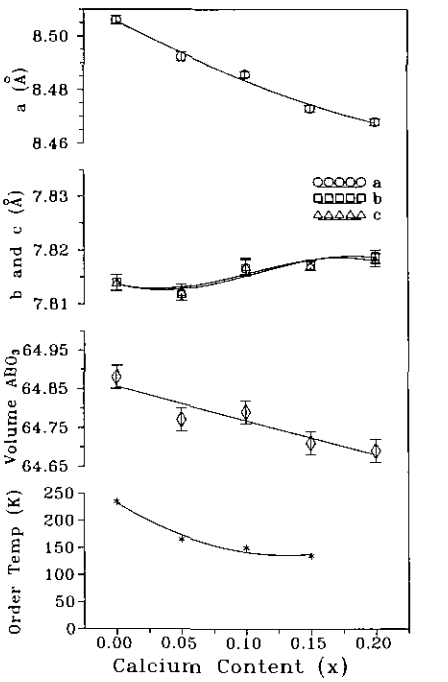

FIG. 7. Lattice constants, volume per perovskite unit (ABO_3), and maximum temperature at which antiferromagnetic order exists versus strontium content for $La_{2-x}Ca_xCuSnO_6$.

An additional factor, owing to the Jahn–Teller ordering of localized Cu $dx^2 - y^2$ electrons, likely contributes to the overall monoclinic symmetry (*18*). When there is an *A–B* size mismatch, as in La_2CuIrO_6 (*19*), the Jahn–Teller ordering coupled with rota-

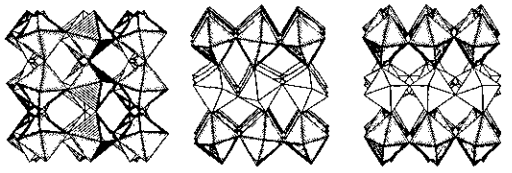

FIG. 8. Metal-oxygen polyhedra for La_2CuSnO_6 viewed down the three primary axes. The sign indicates the relative tilt of octahedra along the indicated axis. Shaded polyhedra are CuO_6 and unshaded polyhedra are SnO_6.

tions of the BO_6 octahedra reduce the symmetry to monoclinic.

Properties

For the composition $La_{2-x}Sr_xCuSnO_{6-x/2+\delta}$, there are three possibilities: (1) strontium is not incorporated into the structure and various phases result, (2) strontium is incorporated into the structure and oxygen defects are created ($\delta < x/2$), or (3) strontium is incorporated into the structure and it oxidizes the compound ($\delta = x/2$, p-type doping). For $x \leq 0.15$, the last occurs, strontium is incorporated into the structure and the compound is oxidized. Evidence for this includes the change of lattice parameters, the lack of impurities in the X-ray diffraction pattern, the large decrease in resistivity, and the overall oxygen content of 6.00. The possibility of oxidation of the copper by the mechanism

$$2Cu^{II} + Sn^{IV} \rightarrow 2Cu^{III} + Sn^{II} \quad (3)$$

is expected to be unfavorable, and Mössbauer results confirm that it does not occur for $x = 0.00$ or $x = 0.15$. Therefore, the tin $5s$ orbitals lie higher in energy than the copper $3d$ manifold as expected.

Structure–Property Relationships

The structural features of $La_{2-x}Sr_xCuSnO_6$ (namely, copper–oxygen planes) are similar to high-temperature cuprate superconductors, yet the physical properties are quite different. The phase remains semiconducting even at strontium concentrations that produce superconductivity in other layered cuprates. We assert that the reason is the interleaved tin-oxygen layers significantly change the crystal chemistry and dramatically alter the electronic structure of the copper–oxygen planes. To determine the effect of crystal chemistry on the structure and properties, we compare the system to the layered cuprate La_2CuO_4. We detail the differences of crystal chemistry, present the Cu d–O $2p$ band region in La_2CuO_4, and examine the effect the interleaved tin–oxygen layers have on the Cu d–O $2p$ band region in La_2CuSnO_6. Finally, we present two models of the electronic structure of La_2CuSnO_6. Calculations of the electronic structures of La_2CuO_4 and La_2CuSnO_6 were performed using the Extended Hückel implementation of tight binding theory (*20*).

1. Crystal chemistry of La_2CuSnO_6 and La_2CuO_4. The crystal chemistry of La_2CuSnO_6 is quite different from La_2CuO_4. In $La_{2-x}Sr_xCuO_4$, the in-plane Cu–O bond lengths decrease approximately 0.02 angstroms, owing to depletion of electrons from the filled lower Hubbard band (described in the next section), and the axial bond lengths (and dz^2 orbitals) are little affected (*21*, *22*). In $La_{2-x}Sr_xCuSnO_6$, the in-plane Cu–O bond lengths *increase* and the axial bond lengths *decrease* approximately 0.03 Å. If the electronic structure of $La_{2-x}Sr_xCuSnO_6$ were similar to $La_{2-x}Sr_xCuO_4$, with increased strontium content we would expect the in-plane bonds to decrease, the axial bonds to be little affected, the antiferromagnetic interactions to diminish, and the compounds to superconduct.

2. Electronic structure of La_2CuO_4. A schematic band structure diagram for La_2CuO_4 appears in Fig. 9a, where we have focused on the Cu d-orbital region. The

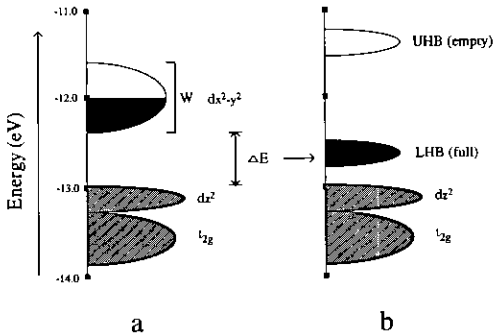

FIG. 9. (a) Schematic band structure diagram (d-orbital region) for La_2CuO_4 before correlation splitting. (b) Schematic band structure diagram after correlation splitting. "UHB" designates upper Hubbard band and "LHB" designates lower Hubbard band.

band formed by overlap of the Cu $dx^2 - y^2$ orbitals with O $2p$ orbitals lies higher in energy than the dz^2 orbitals. In the simplest model (*23*), both lie higher in energy than the Cu t_{2g} band. The splitting of the $dx^2 - y^2$ and dz^2 bands results from the Jahn–Teller instability of the d^9 Cu(II) center. The half-filled band for $dx^2 - y^2$ and the large electron–electron repulsion, U, in the undoped material results in the formation of a Mott–Hubbard (antiferromagnetic) insulator. The $dx^2 - y^2$ band splits into a filled lower (LHB) and empty higher energy band (UHB), with a significant correlation gap between them; see Fig. 9b. Doping this compound with Sr^{2+} relieves the instability of the half-filled band at the copper center by removing electrons from $dx^2 - y^2$ and thus generates a metallic (superconductive) state in $La_{2-x}Sr_xCuO_4$ for $0.05 < x < 0.20$. Within the Hubbard framework, the metallic state is possible in doped compounds when the band width associated with Cu $dx^2 - y^2$/O $2p$ overlap, W, is larger than the electron–electron repulsion, U, or in a mixed-valent system ($W \approx U$) provided W is large enough for small-polaron motion to go to itinerant-electron behavior (*24*).

3. Effect of crystal chemistry on the relative energy of the $dx^2 - y^2$ and dz^2 bands in La_2CuSnO_6. The band structure diagram for the Cu d-orbital region of La_2CuSnO_6 has the same general features as for La_2CuO_4 because both contain d^9 Cu(II); see Fig. 10a. Both contain a half-filled Cu $dx^2 - y^2$ band that lies higher in energy than the dz^2 band, but, in La_2CuSnO_6 three crystal chemical effects conspire to reduce the energy separation between the $dx^2 - y^2$ and dz^2 bands:

(1) A–B size mismatch;
(2) copper–tin size mismatch;
(3) tin–oxygen lattice relaxation caused by introduction of divalent metal atoms (Sr, Ca).

All three decrease the overlap of the Cu $dx^2 - y^2$ and O $2p$ orbitals, which relieves the antibonding character of the half-filled $dx^2 - y^2$ band and reduces its energy (from our tight binding calculation, the energy is reduced from -12.0 eV in La_2CuO_4 to -12.3 eV in La_2CuSnO_6). The three decrease the overlap of the Cu $dx^2 - y^2$ and O $2p$ orbitals in the following manner: the first buckles the Cu–$O_{4/2}$ planes (158–165° in La_2CuSnO_6 compared to 178° in orthorhombic La_2CuO_4), the second elongates the in-plane Cu–O bonds (1.989 Å average in La_2CuSnO_6 compared to 1.907 Å average

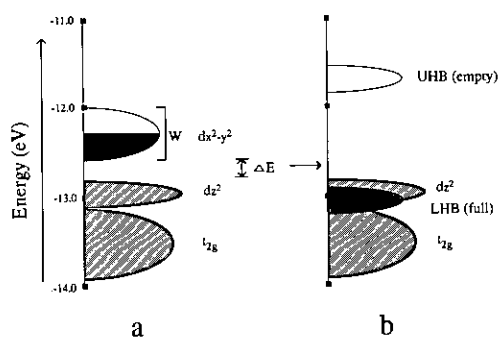

FIG. 10. (a) Schematic band structure diagram (d-orbital region) for La_2CuSnO_6 before correlation splitting. (b) Schematic band structure diagram after correlation splitting. "UHB" designates upper Hubbard band and "LHB" designates lower Hubbard band.

in La_2CuO_4), and the third decreases the A–O bond strength and allows the $SnO_{4/2}$ layers to expand slightly, which places additional tensile stress on the Cu–O bonds. The severely bent copper–oxygen sheets result in a narrower $dx^2 - y^2$ band (0.56 eV compared to 0.81 eV in La_2CuO_4). In addition to the reduction of energy of the $dx^2 - y^2$ band, the first mismatch raises the energy of the dz^2 band. It compresses the axial copper–oxygen bonds approximately 0.02 Å compared to La_2CuO_4, increases the overlap of Cu dz^2 and O $2p$ orbitals, and accentuates the antibonding character of the dz^2 band.

4. Electronic structure of La_2CuSnO_6. When the correlation splitting is introduced, the relative position of the dz^2 and lower $dx^2 - y^2$ (lower Hubbard band) bands is in question, owing to the reduced energy separation between them. The dz^2 band either lies below the lower Hubbard band (model 1, Fig. 9b) or lies between the upper and lower Hubbard bands (model 2, Fig. 10b). Either model can potentially explain the increased in-plane bond lengths, decreased axial bond lengths, and persistence of antiferromagnetic order upon oxidation by strontium.

For model 1, electrostatic factors override electronic effects and lead to an electronic structure similar to that shown for La_2CuO_4; see Fig. 9b. The A–B and Cu–Sn mismatches along with the lattice relaxation prevent the expected decrease in Cu–O bond lengths even though the electrons are removed from $dx^2 - y^2$. The smaller size of copper(III) as compared to copper(II) allows a decrease in the axial Cu–O bond lengths.

For model 2, electrostatic and electronic factors are synergistic. The correlation splitting forces the lower Hubbard band below the filled dz^2 band, shown in Fig. 10b. Upon oxidation of copper, electrons are removed from the dz^2 band, and, because the dz^2 orbitals are included in antibonding interactions with the axial oxygen atoms, the axial Cu–O bond distances decrease. The purely electronic model predicts no change in the in-plane bond lengths or angles because the $dx^2 - y^2$/O $2p$ antibonding interactions are not relieved. However, the b and c lattice parameters increase, thus the Cu–O bond lengths increase and/or the Cu–O planes flatten (*12*). The tin–oxygen lattice relaxation brings about the increased bond lengths and/or the flattened planes.

Regardless of the position of dz^2 with respect to the $dx^2 - y^2$ band, tin has a profound effect on the physical properties. The chemistry of tin prohibits the decrease of the in-plane copper–oxygen bond lengths, which keeps electron–electron correlations, U, larger than the $dx^2 - y^2$ band width, W, a situation that is consistent with an antiferromagnetic semiconductor.

Conclusions

In $La_{2-x}Sr_xCuSnO_{6-x/2+\delta}$, the increase of the b and c lattice parameters (parallel to the copper–oxygen planes) and decrease of the a lattice parameter (nearly perpendicular to the planes) upon addition of strontium is manifested by electrostatic and electronic factors, rather than strictly electronic. The material has been made p-type and progresses from an intrinsic to a doped semiconductor; however, p-type superconductivity does not appear likely in the system because the mismatch between the tin– and copper–oxygen layers elongates the copper–oxygen bonds and keeps the electron–electron correlations larger than the width of the $dx^2 - y^2$ band. The tin is necessary to stabilize the layered arrangement of B cations (*1*), but also appears to be detrimental to superconductivity.

Acknowledgments

This work benefitted from the use of the Intense Pulsed Neutron Source at Argonne National Laboratory. The authors thank R. Hitterman and J. Richard-

son for their assistance. Funding for the neutron time and the authors was provided by the National Science Foundation and the Science and Technology Center for Superconductivity (NSF-DMR-8809854). We gratefully acknowledge B. Dabrowski for the samples annealed under high oxygen pressure, and J. F. Mitchell for important discussions on the electronic structure. We also acknowledge the Northwestern Materials Research Center for support of the X-ray Diffraction Facility (MRL-DMR-8821571).

References

1. M. T. Anderson and K. R. Poeppelmeier, *Chem. Mater.* **3,** 476 (1991).
2. (a) S. Uchida, H. Takagi, K. Kitazawa, and S. Tanaka, *Jpn. J. Appl. Phys.* **26,** L1 (1987); (b) H. Takagi, S. Uchida, K. Kitazawa, and S. Tanaka, *Jpn. J. Appl. Phys.* **26,** L123 (1987).
3. R. J. Cava, R. B. van Dover, B. Batlogg, and E. A. Rietman, *Phys. Rev. Lett.* **58**(4), 408 (1987).
4. Y. Tokuza, H. Takagi, and S. Uchida, *Nature* **337,** 345 (1989).
5. R. J. Cava, B. Batlogg, R. B. vanDover, J. J. Krajewski, J. V. Waszczak, R. M. Fleming, W. F. Peck, L. W. Rupp, P. Marsh, A. C. W. P. James, and L. F. Schneemeyer, *Nature* **345,** 602 (1990).
6. J. T. Vaughey, J. P. Thiel, E. F. Hasty, D. A. Groenke, C. L. Stern, K. R. Poeppelmeier, B. Dabrowski, D. G. Hinks, and A. W. Mitchell, *Chem. Mater.* **3,** 935 (1991).
7. D. B. Wiles and A. Sakthivel, R. A. Young, "Rietveld Analysis Program, Version 9006," School of Physics, Georgia Institute of Technology (1990).
8. R. B. Von Dreele, G. D. Jorgensen, and C. G. Windsor, *J. Appl. Crystallogr.* **15,** 581 (1982).
9. F. J. Rotella and J. W. Richardson, Jr., "Workshop on Neutron Scattering Data Analysis 1986," Chap. 1, IOP, Bristol, UK (1986).
10. A. J. Jacobson, B. C. Tofield, and B. E. F. Fender, *J. Phys. C* **6,** 1615 (1973).
11. $R_{\text{profile}} \equiv 100 \times \Sigma[|(Y_{\text{obs}} - Y_{\text{calc}})|]/\Sigma[|(Y_{\text{obs}})|]$; $R_{\text{weighted profile}} \equiv 100 \times \text{SQRT}(\Sigma[W \times (Y_{\text{obs}} - Y_{\text{calc}})^2])/\Sigma[W * (Y_{\text{obs}})^2])$; $R_{|F|^2} \equiv 100 \times \Sigma[|(I_{\text{obs}} - I_{\text{calc}})|]/\Sigma[|(I_{\text{obs}})|]$; $R_{\text{Rietveld}} \equiv 100 \times \Sigma[|(Y_{\text{obs}} - Y_{\text{calc}})|]/\Sigma[|(Y_{\text{obs}}) - \text{Background}|]$; $R_{\text{expected}} \equiv 100 \times \text{SQRT}(\text{Number of Degrees of Freedom}/\Sigma[W \times (Y_{\text{obs}})^2])$. Y_{obs} and Y_{calc} are the observed and calculated profile intensities at a particular time-of-flight value, respectively, and W is $1/Y_{\text{obs}}$. I_{obs} and I_{calc} are the observed and calculated intensities of each Bragg peak, respectively.
12. The apparent changes of in-plane Cu–O bond are within the error of the neutron experiment. The X-ray diffraction experiments (lattice parameter increase) indicate an average increase of 0.004 Å per Cu–O unit. This increase can result from bond length increase or flattened planes or both.
13. V. M. Goldschmidt, *Str. Nor. Vidensk-Akad. Oslo* **1,** 1 (1926).
14. R. D. Shannon, *Acta Crystallogr., Sect A* **32,** 751 (1976).
15. A. M. Glazer, *Acta Crystallogr., Sect. B* **28,** 3384 (1972).
16. In the notation $(a + b + c)$, "a" refers to the coordination number from the Cu–O plane, "b" to the La–O plane, and "c" to the Sn–O plane.
17. Tin(IV) (0.69 Å) is larger than copper(II) (0.60 Å in-plane). A typical in-plane copper–copper distance in an oxide is 3.8 Å, and a typical Cu–O bond length in the range 1.89 to 1.95 Å. A typical tin–tin distance in an oxide is 4.1 Å, and a typical Sn–O bond length is 2.05 Å.
18. J. B. Goodenough and J. M. Longo, *in* "Landolt–Börnstein, Numerical Data and Functional Relationships in Science and Technology" (K.-H. Hellwege, Ed.), Group III/Vol. 4a, p. 147, Springer-Verlag, Berlin (1970).
19. G. Blasse, *J. Inorg. Nucl. Chem.* **27,** 993 (1965).
20. J. K. Burdett and G. V. Kulkavni, *Phys. Rev. B* **40,** 8908 (1989).
21. J. M. Tarascon, L. H. Greene, W. R. McKinnon, G. W. Hull, and T. H. Gaballe, *Science* **235,** 1373 (1987).
22. M.-H. Whangbo and C. C. Torardi, *Acc. Chem. Res.* **24,** 127 (1991).
23. J. K. Burdett, *Adv. Chem. Phys.*, in press.
24. J. B. Goodenough and J. Zhou, *Phys. Rev. B* **42**(7), 4276 (1990).